PROCEEDINGS, 47th Workshop on Geothermal Reservoir Engineering
Stanford University, Stanford, California, February 7-9, 2022
SGP-TR-223

Radiators or Reservoirs: Heat Budgets in District-Scale Ground-Source Geothermal Exchange Fields

David J. Hart[1], James M. Tinjum[2], Dante Fratta[2], Lauren K. Thomas[3], and Emma L. Carew[2]

[1]Wisconsin Geological and Natural History Survey, 3817 Mineral Point Road, Madison, Wisconsin 53705, USA

[2]University of Wisconsin–Madison, Dept. of Civil and Environmental Engineering, 1415 Engineering Drive, Madison, WI 53706, USA

[3]Invenergy, One South Wacker Drive, Suite 1800, Chicago, IL 60606, USA

Corresponding Author Email: jmtinjum@wisc.edu

Keywords: geothermal exchange, heat pump, reservoir, heat budget

ABSTRACT

Ground-source heat pump systems provide low-cost, sustainable, long-term heating and cooling over a range from single residential homes to district-scale. As the scale of the geothermal system increases from a single ground heat exchange (GHX) boring for a home to several thousand GHXs for a district-scale facility, overheating the exchange field and depleting the geothermal resource becomes a concern. District-scale facilities generally cool their buildings more than heat them, resulting in more heat discharged to the exchange field than removed from it annually. In addition, because thousands of borings are often placed in a single exchange field, the temperature profiles of neighboring GHXs are superimposed, reducing their ability to transmit heat to the field. We are studying a district-scale exchange field in Verona, Wisconsin (USA), and evaluating how district-scale geothermal fields operate to improve their efficiencies. This field and heat pumps supply heating and cooling for a campus of approximately 10,000 employees. We collected energy usage and geologic data while monitoring temperature time series to determine the geothermal field's heating budget. That budget consists of (1) heat from the campus moved into and out of the field by the GHXs, (2) changes in heat stored in the field, and (3) heat flow into and out of the field into the surrounding rock and air. This budget allows us to understand how the field is behaving. If the field is a reservoir, then the heat flow from GHXs should equal the change in heat storage with little flow out of the field into the environment. If the field is a radiator, then the heat flow from the GHXs should equal the heat flow from the field into the surrounding rock and atmosphere with little change in the heat stored in the field. Results suggest that the field initially behaved as a reservoir while the temperature of the rock increased during the initial conditioning process. After this initial one- and one-half years, the field is shifting towards acting more like a radiator, likely due to a greater temperature difference between the field and the surrounding rock and air. The geometry of the field and BHXs and the imbalanced heating and cooling loads will require that the field be routinely reconditioned or cooled. It is receiving more heat than it can dissipate, as indicated by the increasing field temperatures, and will likely need to be routinely conditioned by water from surface water reservoirs to maintain cooler temperatures and efficiency over the long-term use of the field.

1. INTRODUCTION

Ground-source heat pumps (GSHP) are low enthalpy systems used for space heating and cooling with low primary energy consumption compared to conventional fossil fuel temperature control. As a result, GSHP systems benefit from low emissions associated with their operation, with 33-50% CO_2 emissions savings globally (Fridleifsson 2008). In addition, ground/geothermal heat exchange (GHX) systems can expand a wide range of application scales, ranging from small residential systems to large-scale systems supporting multiple buildings with hundreds of GHX borings in a field (Siliski et al. 2016). As a result, district-scale systems can be highly competitive with other space heating fuel sources, and geothermal often shows itself to be one of the lowest cost alternatives (McCabe et al. 2019). However, some district-scale systems do not perform as designed. This problem is often due to imbalanced heating and cooling loads with more heat added to the system than is taken out. As a result, the field overheats, and its utility is diminished. Several operations have encountered these issues, including geothermal facilities at Ball State University, West Chester University, and the Wisconsin Institute for Discovery at the University of Wisconsin (Florea et al. 2017, Herrera et al. 2018). Tools to avoid this issue are needed to better manage geothermal heat exchange (GHX) fields.

We propose that heat budget development is essential to sustainable GHX field management. A heat budget (Fig. 1)

$$Q_{source} + Q_{dissipated} = \Delta Q_{storage} \quad (1)$$

is the sum of the heat injected or withdrawn from the field, Q_{source}, the heat flowing into or out of the field to the surrounding environment, $Q_{dissipated}$, and is equal to the change in the amount of heat stored in the field, $\Delta Q_{storage}$. Knowledge of any two terms in this equation is sufficient to estimate the third. The field is a reservoir if the dissipated heat is much less than the change in stored heat, and the geothermal field behaves as a radiator if the dissipated heat is much greater than the change in stored heat. Understanding whether the geothermal field acts as a reservoir or a radiator allows for effective, sustainable management.

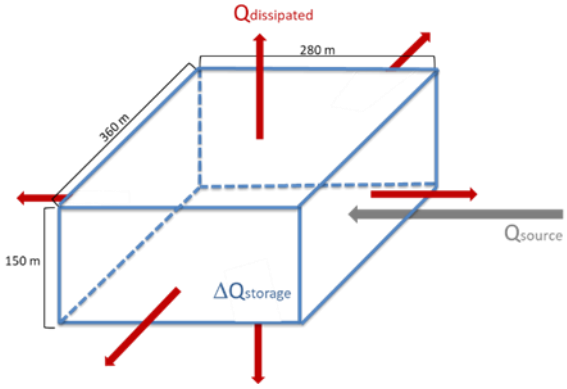

Figure 1: Definition of geothermal field heat budget.

We tested this concept at Epic Systems' (Epic) GSHP system in Verona, Wisconsin, a district-scale system with over 6000 GHX wells. At the site, we installed and monitored a fiber-optic (FO) distributed temperature sensing (DTS) array for more than six years after the district-scale geothermal field was put into operation. FO DTS arrays obtain temperature profiles along several kilometers of fibers (Tyler et al. 2009). While FO DTS technology is often used for short-term monitoring and to characterize the vertical distribution of thermophysical properties during a thermal response test (Acuna and Palm 2013, Beier et al. 2012, Fujii et al. 2009), long-term FO DTS monitoring has provided insight into this GHX field's operation and efficiency (McDaniel et al. 2018b). While numerical modeling can be used to predict *in situ*, three-dimensional heat flow in a large GHX field (Raymond and LaMarche 2013, Özdoğan Dölçek et al. 2016), long-term temperature measurements and the thermal properties of the borefield rock and sediment can more accurately be used to calculate the change in the borefield heat storage over time. Given Epic's cooling-dominated heat load, quantifying the amount of heat independently exiting the borefield allows for an in-depth understanding of how "leaky" the GHX reservoir is. Furthermore, the heat budget assists with the analysis of the GHX field operation to make better-informed long-term operational decisions. This analysis provides a more comprehensive alternative to the GHX penalties analysis used to design and monitor field performance.

2. BACKGROUND

2.1 Project Site

Epic is an electronic health records company that makes software for medical groups, hospitals, and integrated healthcare organizations. Epic is a leader in energy-efficient and cost-effective commercial building design that is environmentally responsible and sustainable. Epic's commitment to energy efficiency and sustainability is evident with Epic's private photovoltaic installation (1.75 MW) and wind turbine farm (9.9 MW). In addition, Epic has invested in geothermal reservoir fields to heat and cool their campus fully. Over the 15 years of operating geothermal reservoir fields, Epic achieved extensive knowledge about the nature of district-scale geothermal systems. This working knowledge allows the development of best practices regarding thermal storage via geothermal heat exchange. The 10,000-person Epic campus in Verona, Wisconsin, has 6,100 in-service GHX wells (up to 152-m depth) located across four separate GHX fields with an existing capacity of 42 $MW_{thermal}$—one of the largest shallow, low-temperature GHX systems in the world (Fig. 2). With additional closed-loop exchanges in a 2.2-ha stormwater management pond and an 8.5-ha, 14-m-deep Quarry Lake, the total capacity reaches 92 $MW_{thermal}$. The thermal reservoirs provide all heating and cooling needs, hot water heating, and ancillary services such as snowmelt operations and underground parking heating. In addition, this site offers a *natural laboratory* with research advantages. The facility is monitored to allow the proper evaluation of the energy balance; includes complex, near-surface geology; and Epic innovatively seeks to enhance the system's performance and sustainability in its operation.

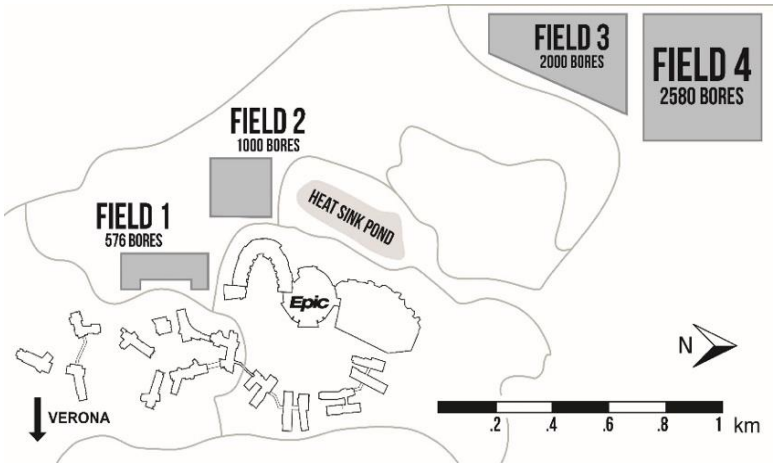

Figure 2: Epic's campus includes four geothermal fields, a cooling pond, and a quarry reservoir (1 km northeast of Field 4).

2.2 Site Geology

The geology of the Epic's geothermal fields is typical of southern Wisconsin, and representative of the soils and lithologies often encountered in the upper Midwest of the United States. Borehole logging captured information about the geology at the site of Field 4. Fig. 3 presents a generalized geologic section for Epic's geothermal Field 4. There is approximately 10 m of fill and glacial till, mostly gravel and sand, over bedrock. Beneath this overburden, there are layers of bedrock lithology beneath this overburden, including limestone and sandstone, which is underlain at the bottom by the Eau Claire shale. The water table is present at a depth of about 23 m. The formations' thermal properties were measured on core samples and presented in Table 1 (Meyer 2013). The Eau Claire Formation shale acts as an aquitard, preventing groundwater flow vertically at the base of the geothermal Field 4 and was not penetrated by the GHX wells. The different lithologies' hydraulic conductivities are expected to result in differential advective flow and heat transport out of the field. Also expected to affect the advective heat transport at this site significantly are the voids in the Prairie du Chien observed at similar depths in multiple boring in geothermal Field 4. These voids are shown in Fig. 4 and are observed in multiple borings in Field 4. The Tunnel City Formation acts like a leaky aquitard. It provides some hydraulic separation between the overlying rock and sediment and the Wonewoc Formation. The shallow piezometers indicate groundwater flow is generally to the southwest in the field in the Tunnel City Group and above, while the deep piezometers indicate groundwater flow in the Wonewoc is to the east during pumping by a nearby municipal well and to the south when the well is not pumping.

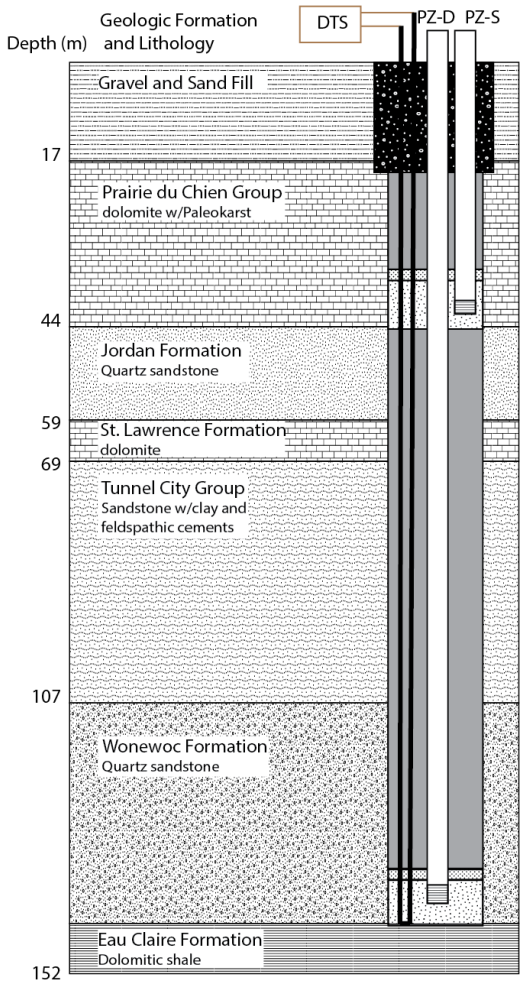

Figure 3: Generalized geology and typical well observation field configuration for Field 4 (modified after McDaniel et al. 2018b).

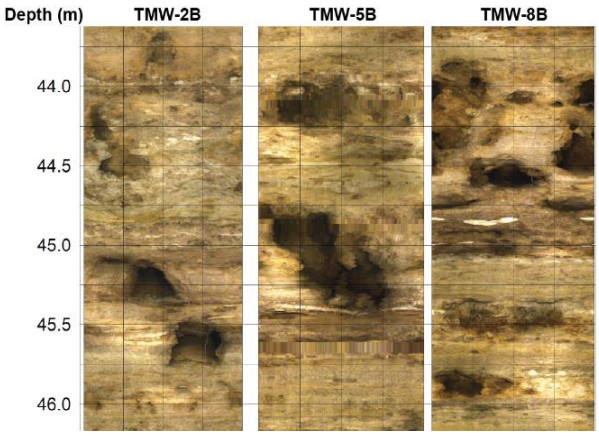

Figure 4: Optical borehole images showing large-scale conduits and voids near the base of the Prairie du Chien Group dolomite.

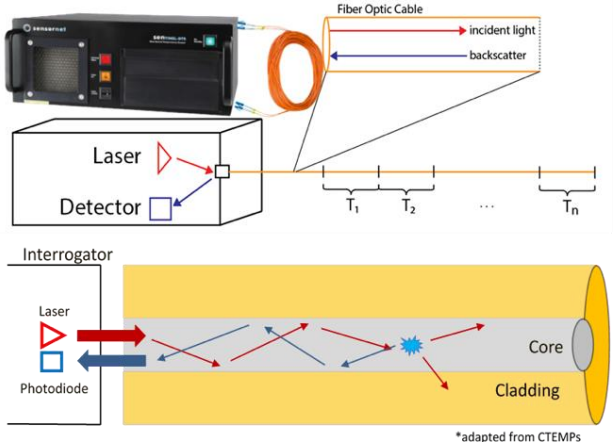

Figure 5: Schematic of the operation of the FO-DTS array. The Raman backscatter signals from different sections of the FO is used to created temperature profiles along the length of the fiber.

3. MATERIALS AND METHODS

Our team installed an array of piezometers and FO DTS in and around geothermal Field 4 to investigate subsurface heat flow response and mechanisms. Fig. 3 shows the typical installation configuration of the temperature monitoring wells. We have been monitoring field performance, including the energy sent into the borefield, since 2015. The piezometers are equipped with a data logger to measure the piezometric surface and water temperature over time. A Sensornet Sentinel DTS-LR interrogator (Fig. 5) with a 16-channel multiplexor was placed in a subsurface vault on the east side of Field 4 (Fig. 6). This interrogator can provide 0.01°C temperature resolution and 1-m spatial resolution over each of these loops. McDaniel et al. (2018a) developed a dynamic calibration method to interpret the DTS data collected at Field 4. Accuracy of calibrated temperatures varied over time (0.05–1.0 °C) with a long-term average of 0.36 °C. The FO DTS loops are sensors that monitor the temperature profile with depth in the temperature monitoring wells, TMW 1B through 8B. In these wells the FO loops grouted in direct contact with the ground. Temperature monitoring wells TMW 4B, 7B, and 8B are also equipped with a piezometer screened in a shallow aquifer and a piezometer screened in a deep aquifer.

3.1 Heat Budget Terms

The heat injected into the field by the BHXs from the Epic's facilities, Q_{source}, and the change in heat storage in Field 4, $\Delta Q_{storage}$, can be calculated using the collected data. The resulting term of heat lost or dissipated to the surrounding environment, $Q_{dissapated}$, is then estimated by subtracting the heat from the source injected or withdrawn by the BHXs from the change in heat storage, $\Delta Q_{storage} - Q_{source}$.

3.2 Change in heat storage

The change in heat storage was estimated using the FO DTS temperature data in each of the six temperature monitoring wells located inside Field 4, TMW 1B–6B (Fig. 6), thermal properties of the lithologies encountered in each of the sentry wells, and the dimensions of the field.

$$\Delta Q_{storage} = \sum_{i=1}^{n} \Delta T_i \rho_i \, Cp_i \, \Delta z_i \, \Delta x \, \Delta y \qquad (2)$$

Where $\Delta Q_{storage}$ [J] is the change in heat storage for one of the six sections of Field 4, i is the depth interval count from 1 to n, ΔT_i is the temperature change since the field section was in operation at the *i-th* depth[C], ρ_i is the rock or sediment density at the *i-th* depth [kg/m^3], Cp_i is the specific heat capacity [J kg^{-1} K^{-1}], $\Delta z_i$is the thickness at the *i-th* depth [m], and Δx and Δy are the horizontal dimensions of the field section [m]. The maximum depths of the six field sections ranged from 130 m to 150 m. Table 1 shows the dry and saturated thermal properties of the rock and sediment in the six sections. The depths of the rock and sediments varied from section to section and thermal properties were thus assigned according to the rock and sediment logs collected at each of the sentry wells. A generalized example is shown in Fig. 3.

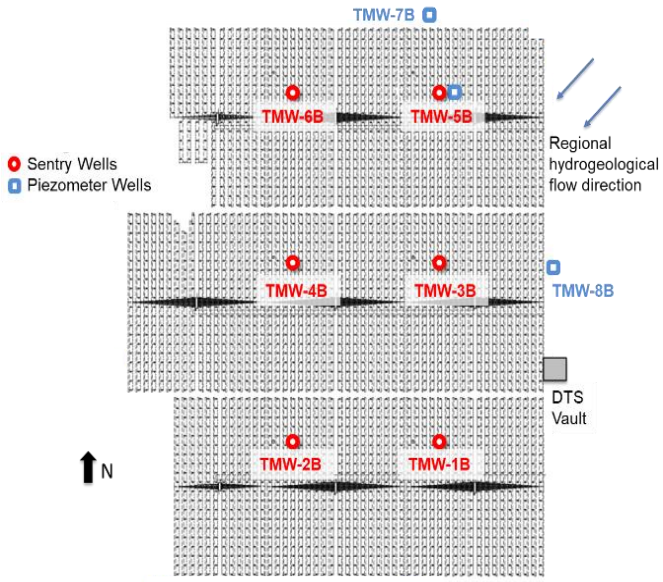

Figure 6: Location of the high-resolution and long-term TMWs in Field 4. The location of the field within Epic's campus is presented in Fig. 2.

Table 1. Porosity (ϕ), specific heat (Cp) and densities (ρ) under dry and saturated conditions, and the volumetric heat capacity (Cv) of the geologic units at Field 4 used to calculate $\Delta Q_{storage}$.

Geologic Unit	ϕ [%]	Dry Cp [J kg^{-1} K^{-1}]	Dry ρ [kg m^{-3}]	Saturated Cp [J kg^{-1} K^{-1}]	Saturated ρ [kg m^{-3}]	Volumetric Cv = Cp ρ [J m^{-3} K^{-1}]
Gravel and Sand	15	**800**	**1800**	1280	1950	$1.44 \cdot 10^6$
Prairie du Chien Dolomite	5	**832**	**2570**	**899**	**2620**	$2.29 \cdot 10^6$
Jordan Sandstone	22	821	2300	**1070**	**2520**	$2.70 \cdot 10^6$
St. Lawrence Dolomite	5	872	2740	**881**	**2790**	$2.46 \cdot 10^6$
Tunnel City Sandstone	13	891	2540	**998**	**2670**	$2.66 \cdot 10^6$
Wonewoc Sandstone	10	870	2310	**1060**	**2410**	$2.55 \cdot 10^6$

These table values were derived using previously measured values from core samples for the specific formation of interest (Meyer 2013, Walker et al. 2015). Those samples were measured under unsaturated dry conditions. However, the geologic units are all saturated except for the Sand and Gravel and the uppermost 10 m of the Prairie du Chien dolomite. The dry density was corrected for saturated conditions using Eq. 3 using the density of water and the measured porosities.

$$\rho_{sat} = \rho_{dry} + \phi \rho_{water} \qquad (3)$$

The specific heat under saturated conditions was calculated using Eq. 4 and the calculated saturated densities.

$$Cp_{sat} = \frac{Cp_{dry} \cdot \rho_{dry} \cdot (1-\phi) + Cp_{water} \cdot \rho_{water} \cdot \phi}{\rho_{sat}} \qquad (4)$$

The values shown in bold in Table 1 were used in Equation 2 to calculate the change in heat storage for each of the six sections. The dry and saturated values of the Prairie du Chien dolomite were used with the appropriated depths since the water table is present within that formation at this site.

Temperatures in each of the sentry wells were recorded at 1-m intervals and initially every 15 min. The time interval was increased to approximately 2 h 20 min after the first 3 months of operation to reduce amount of data. Each sentry well recorded around 150 temperatures 32,210 times for a total of nearly 5 million temperature measurements for each sentry well. Those data are shown in Fig. 7 with air temperature for sentry well TMW 1B from the period of May 2015 to September 2021. In this plot, time is on the x-axis, depth is on the y-axis, and temperature is shown as a color flood ranging from 9 °C to 18 °C. Areas of no data are shown in white. These occurred for several reasons, including instrument malfunction during the COVID-19 pandemic and power outages in the vault where the instrument is housed.

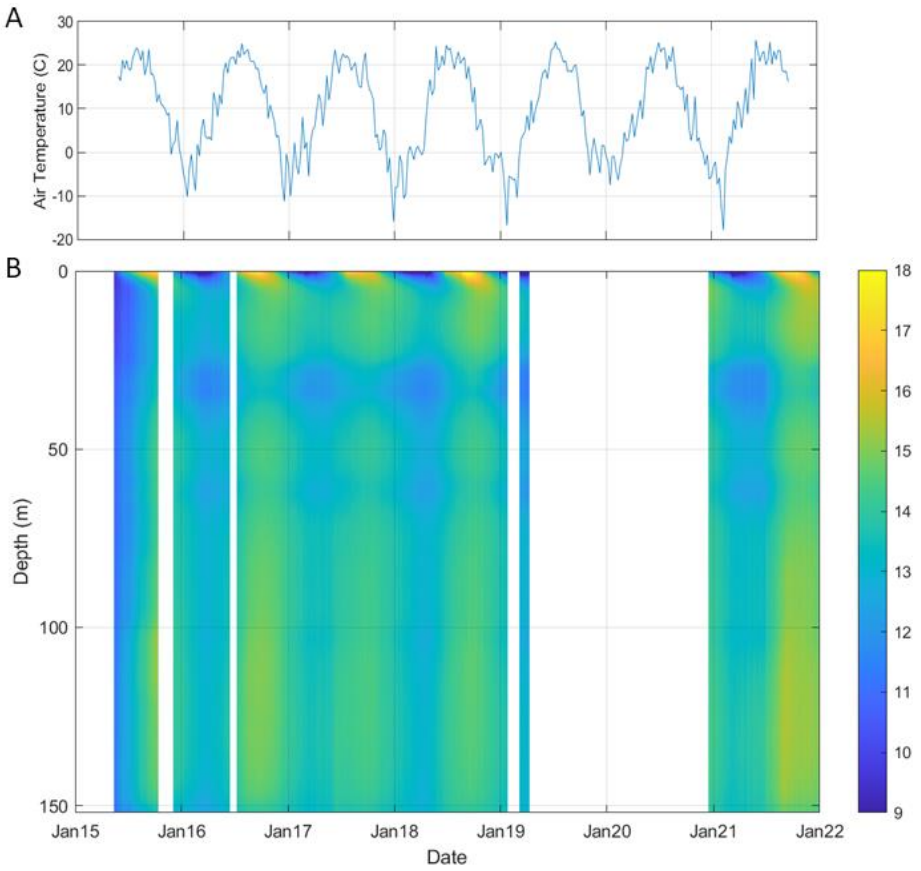

Figure 7: (A) Local air temperature and (B) TMW 1B temperature distribution versus time and depth for January 2015 to January 2022. The color scale represents the temperature in degrees Celsius.

We can see how the field temperatures at TMW 1B vary over the study period and annually. The sentry well temperatures are initially between 9 °C and 11 °C, prior to the field being in use as seen at the left-hand side of the plot in blue. As heat is injected into the field, the sentry well shows the field warming to around 14 °C shown as light yellow and then cooling. This warming and cooling is an annual signal varying with the load from the facility. Another annual signal is present in the shallow sediments to a depth of about 10 m. Here air temperature is controlling these shallow temperatures with the warmest shallow temperatures occurring in the summer and the coldest shallow temperatures occurring in the winter. Other significant temperature patterns with depth are discussed in McDaniel et al. (2018b). For example, the cooler temperatures at 30 m correspond the karst interval shown in Fig. 3.

The change in temperatures for all six sections was calculated from weekly averages of the data for each sentry well. The initial week was used as the starting values and the subsequent weekly averaged temperatures were subtracted from that initial week. That data is shown in Fig. 8 for TMW 1B. The annual cycles are readily apparent in this plot as well. The intervals are in 1-°C increments and go from least change, light blue to most change, yellow. Only the upper 10 m has temperatures cooler than the initial temperatures. The sentry well shows temperature increases from 2 °C to 4 °C over most of its depth. The latest temperature changes in late 2021 are the largest since the field was put into use.

The change in heat storage for each of the six sections was calculated using Eq. 2. The heat change with depth was summed for each of the week-averaged temperature changes to give the overall heat change for the section. Sections with sentry wells TMW 1B and TMW 2B were put into production in May 2015 with the remaining four sections with sentry wells TMW 3B through TMW 6B put into production in December 2015. These results are shown in Fig. 9 as heat change in each section plotted over time. It is interesting to note that TMW 1B and TMW 2B both have similar heat changes in the early times but have diverged so that TMW 1B has only about 60% of the change in heat storage compared to TMW 2B. The reasons for this are uncertain and an area of future investigation. The depths and lithologies are similar between the two wells while the temperatures in TMW 1B are much cooler than that in TMW 2B. We suspect it may be due to groundwater flow cooling TMW 1B more than the other sections and not due to thermal properties or volumes. We also observe that the other sections quickly warmed and had heat changes similar to TMW 2B within the first year of operation. The sum of these six sections gives the change in heat storage for Field 4 and is one of the terms for the heat budget. This sum assumes that there are not significant changes in temperature or lithology across an individual section. While this assumption is not likely to be met, it does allow a quick estimate of heat storage. We are planning a more in-depth analysis using a coupled heat and groundwater advection/conduction model that uses these data as targets.

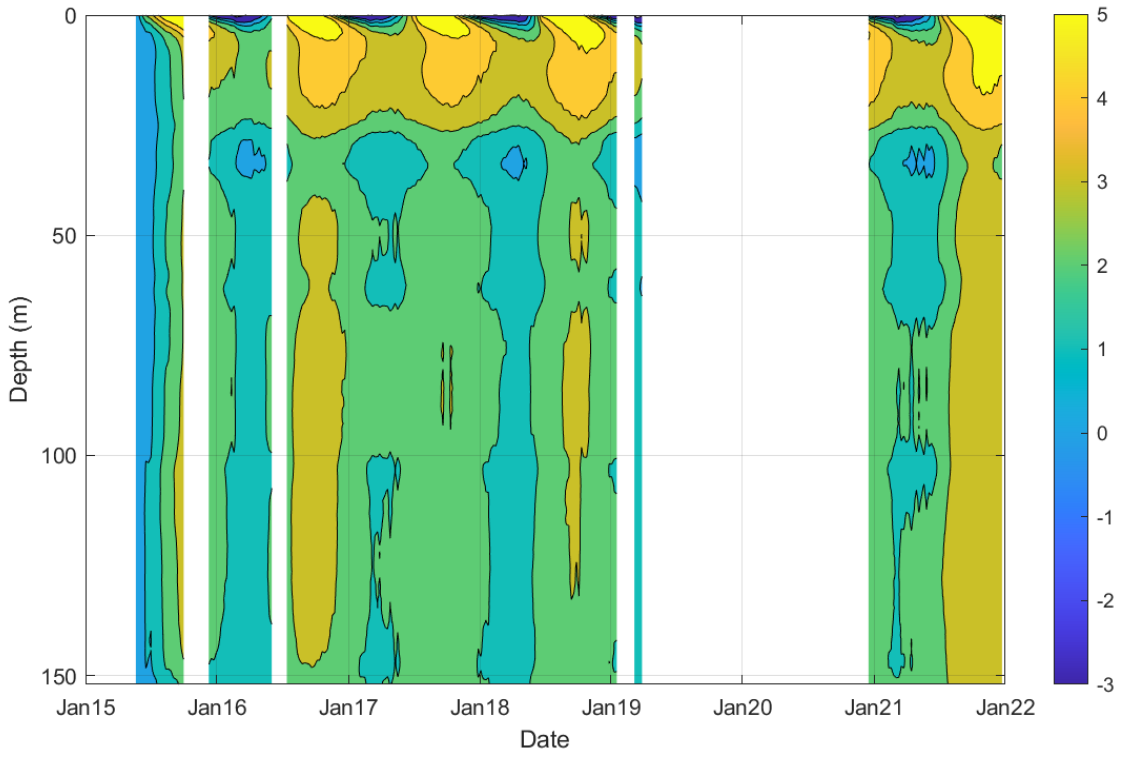

Figure 8: TMW 1B temperature change versus time and depth for January 2015 to January 2022. The color scale represents the temperature in degrees Celsius.

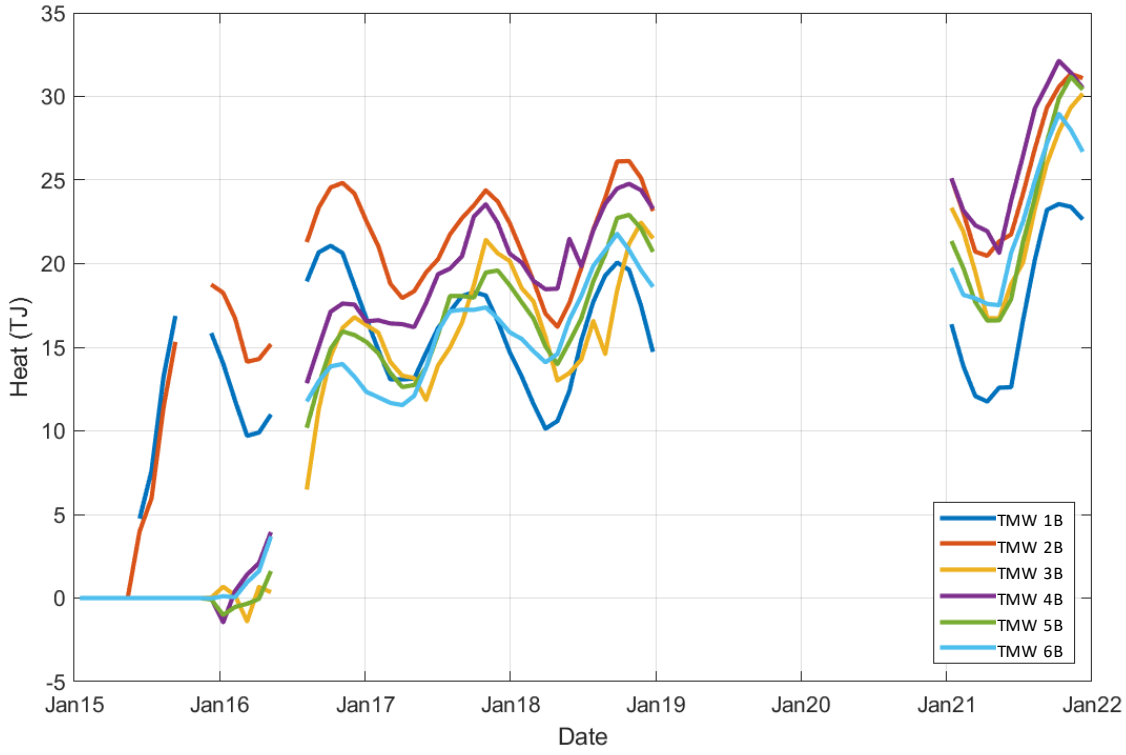

Figure 9: Evolution of heat change in Epic's Field 4 as captured by sentry wells TMW 1B through TMW 6B.

3.3 Heat from the source

The heat from the source was calculated using data supplied by Epic Systems. They have installed a Cimplicity system that records heat transfer and use in different areas of their campus. Piped water is used to transport heat to and from Field 4. The water is piped through supply and return lines and distributed to the GHX wells through a series of manifolds. The water supply and return temperatures and flow rates from the facility to Field 4 are recorded at 15-min intervals. These data allow us to determine heat flow to and from Field 4 using Eq. 3.

$$Q_{source} = (T_{supply} - T_{return})\mathrm{Q}_{pump}\,\rho_{water}\,Cp_{water}\,\Delta t \tag{5}$$

where Q_{source} is the heat transferred into or out of Field 4 from the campus [J], T_{supply} and T_{return} are the supply and return temperatures of the supply and return water, respectively, to the Field 4 BHX wells [C], Q_{pump} is the pumped water flow rate [m^3/s], ρ_{water} is the density of water [kg/m^3], Cp_{water} is the specific heat of water [J kg^{-1} K^{-1}], and Δt is the period of the temperature and flow measurements [s]. We averaged and summed the data by month.

4. RESULTS

4.1 Heat Budget

The change in heat storage in Field 4 and the heat from the source were interpolated so that they were on a single time scale. The resulting estimate of the heat lost or dissipated from Field 4 was calculated by subtracting the heat from the source from the change in heat storage. The three terms of the heat budget are shown in Fig. 10 as a cumulative heat budget from the time since the field was put into use in May of 2015. Overall Q_{source} is increasing over time, indicating that the field is receiving an imbalanced load where more heat is injected into than extracted from the field. This trend was modeled by Özdoğan-Dölçek et al. (2017). Since May 2015, around 320 TJ of heat has been injected into the field. Seasonal reductions occur during the colder months of December, January, and February, as heat is withdrawn from Field 4 for heating of the facility but during the other months, heat from the facility is injected into Field 4. For the first one and one-half years Q_{source} was at a higher rate of heat moving into the field. Since that time the rate has slowed and remained relatively constant. The average power flow into the field over the time shown as the best fit line is 1.1 MW over the last five and one-half years of the field operation.

The change in heat storage of Field 4, $\Delta Q_{storage}$, also increased rapidly in the one and one-half years after the field was put into use. The rate of change slowed and $\Delta Q_{storage}$ seems to be slowly increasing. The variation in heat storage tracks the Q_{source} term closely, indicating little lag between the two terms. The heat stored in Field 4, $\Delta Q_{storage}$, has increased to around 120 TJ for an average power flow stored in the field of 0.3 MW over the last five and one-half years of field operation.

The cumulative heat dissipated, $Q_{dissapated}$, out of Field 4 is negative, showing that the heat is moving out of Field 4 and into the surrounding environment. The total out flows are just over 200 TJ over the lifetime of Field 4 for an average of about 0.8 MW of heat energy being lost to the surrounding environment over the last five and one-half years. The smaller slope in the first one and one-half years indicates the field was dissipating relatively less heat than at later times.

5. DISCUSSION

5.1 Power into and out of Field 4

The cumulative energy budgets presented in Fig. 10 provides insights into shorter time scales by considering the rate of heat change or power. This is done by calculating the slopes of the energy over time curves with time. Fig. 11 shows the power, averaged monthly, into and out of Field 4. This plot shows that the highest rate of energy moved peaks during the summer months when between 5 and 10 MW are moving into Field 4 from the facility. The heat storage has a slightly smaller magnitude peak at the same time for the years with complete data. The heat dissipated power is generally negative at around 1–2 MW, suggesting heat flow out of Field 4. However, two positive excursions occur during the Fall of 2017, Fall of 2018, and Fall of 2021 when the source and field storage powers are both decreasing, suggesting heat inflow from the environment into Field 4 for those brief times.

5.2 Reservoir or Radiator

A field is a reservoir if the change in heat stored in the field is nearly the same as the heat moved into the field. The field is a radiator if the heat dissipated is nearly the same as the heat moved into the field or if the change in heat storage is near zero. Fig. 12 shows the percentage of $\Delta Q_{storage}$ to Q_{source}. A percentage near zero indicates that the field is a radiator while a percentage close to 100% is a reservoir. Since this plot is based on the cumulative energy budget, it represents the long-term state of the field. It appears that the field is acting as both a radiator and reservoir with a percentage of 40% to 50% of $\Delta Q_{storage}$ to Q_{source}. The field initially had a much higher percentage of heat stored at 70%. That high percentage quickly decreased, and a slight long-term downward trend is apparent, suggesting that the field is trending towards behaving as a radiator over time. It may be that as the temperature difference between the field and the environment increases, more heat is dissipated. This mechanism would provide a weak check on runaway temperatures in geothermal fields. Field temperatures will still increase as Q_{source} increases but not at the same rate. The field operations will need to be adjusted so that enough heat is stored in the field to supply heat during the winter months but while maintaining a low enough field temperature so that the efficiency of the heat pumps is not significantly impacted during the spring, fall, and summer months.

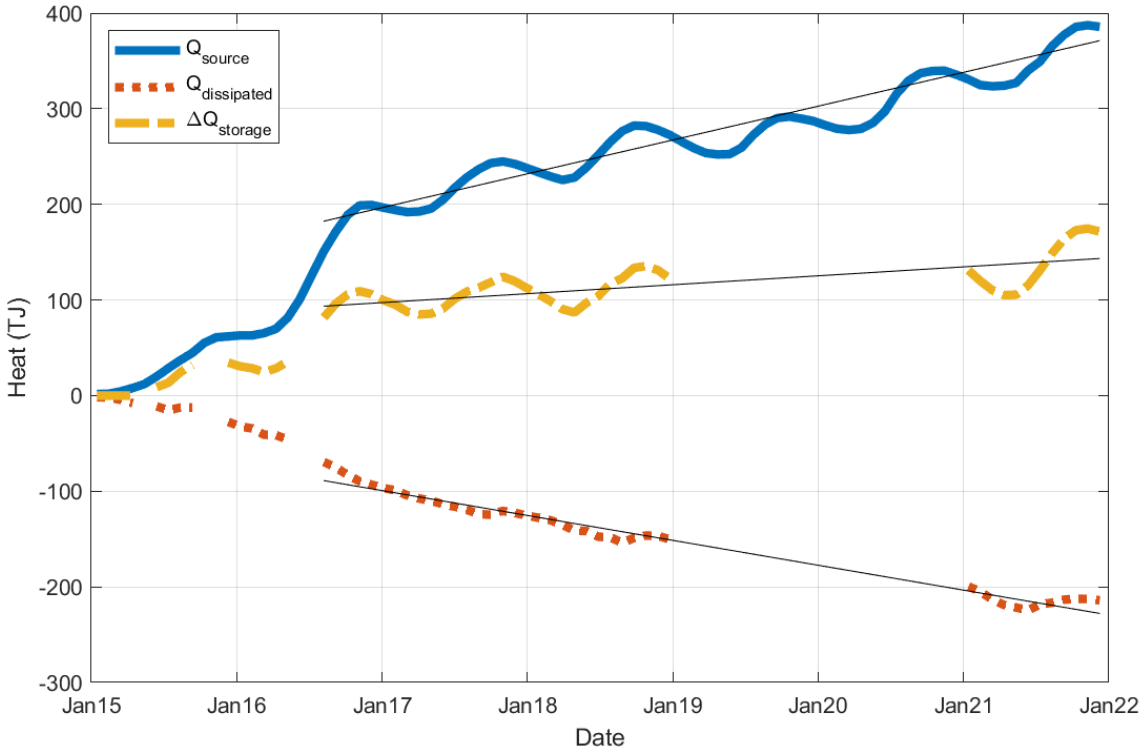

Figure 10: Cumulative heat budget from the time since Field 4 was put in service.

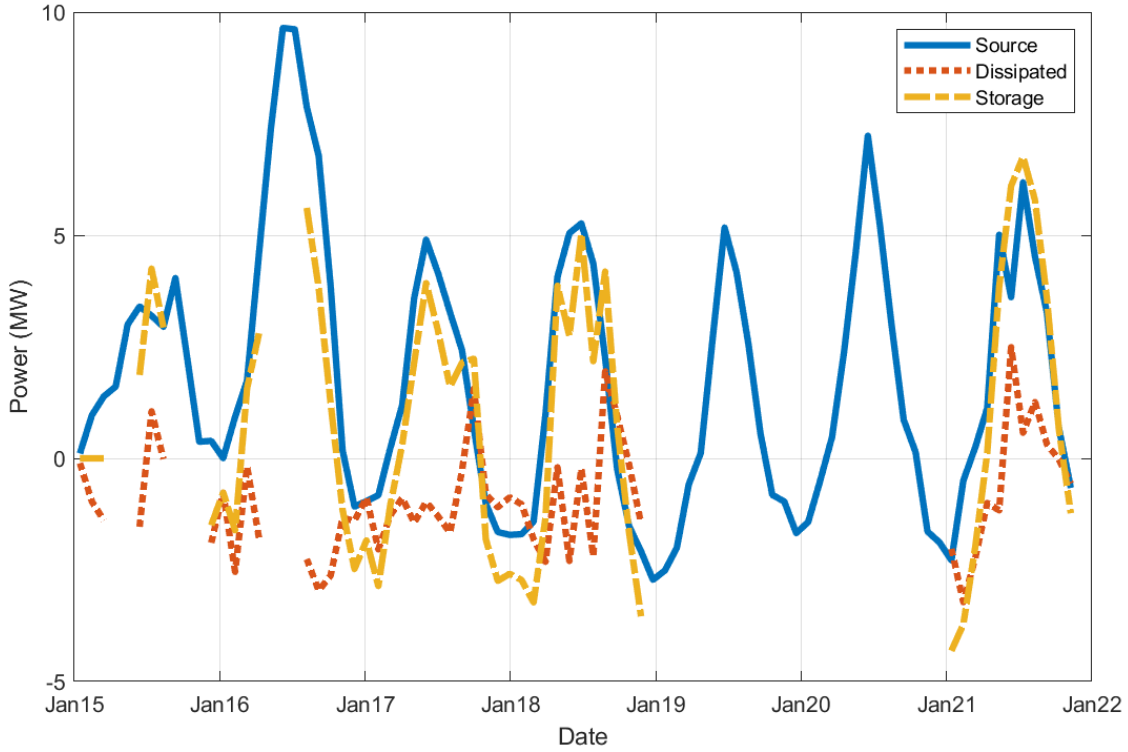

Figure 11: Power variation of input (source), dissipated and stored heat in Field 4.

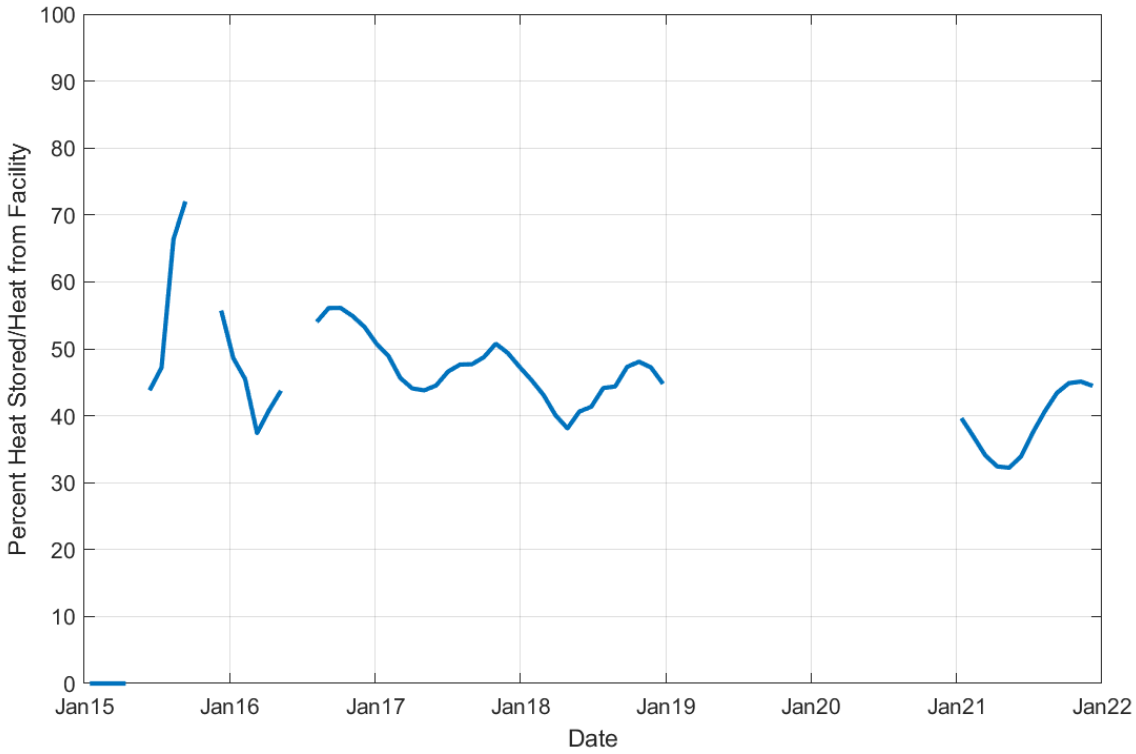

Figure 12: Reservoir or radiator – the time history of $\Delta Q_{storage}$ to Q_{source} percentage for Field 4.

5.3 Design Implications

Field design has many different components and use of a heat budget can help inform design decisions. For example, Q_{source}, or the rate at which the field can accept and discharge heat to the facility depends on borehole length, heat exchanger grout and type, the number of boreholes, temperature difference between the field and the source fluid, and the thermal diffusivity of the field geology. These parameters are the usual focus of field design. However, the rate at which heat can dissipate, $Q_{dissapated}$, depends on the surface to volume ratio of the field, the thermal conductivity of the surrounding geologic materials, groundwater flow direction and magnitude, and the temperature difference between the field and external areas including those on top and bottom. The change in heat storage, $\Delta Q_{storage}$, depends only on the field volume and specific heat of the geologic materials. If the designer can anticipate that the heat load will be unbalanced, they can then design the field appropriately. For example, it will do little good to change the density of the GHX borings or use high thermal conductivity grouts if the field is expected to overheat. However, an increase the field surface to volume ratio would provide more opportunity for heat transfer and reduce overheating, as would alignment of the field perpendicular to groundwater flow to maximize groundwater advection of heat. The geometry of Field 4 is such that the largest surface areas are the top and bottom of the field. The larger area increases heat transfer. Field design should account for field geometry and vertical heat transfer into the atmosphere, not just lateral flow in the subsurface.

6. CONCLUSIONS

We recorded source heat placed into or withdrawn from a district-scale GHX field (and the change in heat storage of the GHX field) to provide a measure of heat dissipated to or from the surrounding environment. These three components form a heat budget that give a useful measure of whether the field is storing or dissipating heat. For many district-scale geothermal fields, the load or heat source to the field is unbalanced (Florea et al. 2017, Herrera et al. 2018). This unbalanced load can cause the field to overheat and reduce the system efficiency. A heat budget provides a measure of the field health beyond supply and return line temperatures since it quantifies the how the heat energy is partitioned between storage and dissipation. This information can then be used to more efficiently remediate the field temperatures or operate the field at a more informed tradeoff between extra heat stored in the field for use during cooler weather and lower field temperatures to improve the heat pump efficiencies during warmer weather. A more accurate budget could be estimated using a coupled advection diffusion model of the heat flows in and around the field and this should be considered for district-scale fields. A heat budget analysis also makes clear that field geometry and orientation with respect to groundwater flow are more important for long-term sustainable field management than GHX boring spacing or grouting. Those components are important, but only for improving how quickly heat can be moved into the field from the source, not for decisions about storing or dissipating heat.

7. ACKNOWLEDGEMENTS

The authors would like to acknowledge Epic Systems Corporation for their generous contributions of time, talent, and resources in the ongoing development of this research. The Morse Company, General Heating and Air Condition Inc., MEP Associates, JP Cullen, and Teel Plastics all donated their expertise, without which, this research would not have been possible. We acknowledge the National Science Foundation for sponsoring undergraduate research opportunities during the early phases of this project under Award # 1156674. We thank

Adam McDaniel (Westwood Professional Services) for preparing the initial Matlab code to process and calibrate FO DTS data and Larue Fuentes (UW–Madison) for carrying this analysis forward. Any opinions, findings, and conclusions or recommendations expressed in this material are those of the authors and do not necessarily reflect the views of the funding organizations.

8. REFERENCES

Acuña, J. and Palm, B.: Distributed Thermal Response Tests on Pipe-in-pipe Borehole Heat Exchangers. Applied Energy, 109, (2013), 312–320.

Beier, R., Acuña, J., Mogensen, P., and Palm, B.: Vertical Temperature Profiles and Borehole Resistance in a U-tube Borehole Heat Exchanger. Geothermics, 44, (2012), 23–32.

Florea, L.J., Hart, D., Tinjum, J.M., and Choi, C.: Potential Impacts to Groundwater from Ground-Coupled Geothermal Heat Pumps in District Scale. Groundwater, 55, (2017), 8–9.

Fridleifsson, I.R.: The Possible Role and Contribution of Geothermal Energy to the Mitigation of Climate Change. IPCC Scoping Meeting on Renewable Energy Sources. Luebeck, Germany. (2008).

Fujii, H., Okubo, H., Nishi, K., Itoi, R., Ohyama, K., and Shibata, K.: An Improved Thermal Response Test for U-tube Ground Heat Exchangers Based on Optical Fiber Thermometers. Geothermics, 38(4), (2009), 399–406.

Herrera, C., Nellis, G., Reindl, D., Klein, S., Tinjum, J.M., and McDaniel, A.: Use of a Fiber Optic Distributed Temperature Sensing System for Thermal Response Testing of Ground-Coupled Heat Exchangers. Geothermics, 71, (2018), 331–338.

McCabe, K., Beckers, K., Young, K.R., and Blair, N.: GeoVision Analysis Supporting Task Force Report: Thermal Applications—Quantifying Technical, Economic, and Market Potential of Geothermal District Heating Systems in the United States. Golden, CO: National Renewable Energy Laboratory. NREL/TP-6A20-71715. (2019).

McDaniel. A., Fratta, D., Tinjum, J.M., and Hart, D.: Long-term District-scale Geothermal Exchange Borefield Monitoring with Fiber Optic Distributed Temperature Sensing. Geothermics, 72C, (2018b), 193–204.

McDaniel. A., Tinjum, J.M., Hart, D., and Fratta, D.: Dynamic Calibration for Permanent Distributed Temperature Sensing Networks. IEEE Sensors Journal, 18(6), (2018a), 2342–2352.

Meyer, L.: Thermophysical Properties of Wisconsin Rocks for Application in Geothermal Energy (Master's Thesis). University of Wisconsin-Madison, Madison, Wisconsin. (2013).

Özdoğan Dölçek, A., Atkins, I., Harper, M.K., Tinjum, J.M., and Choi, C.Y.: Performance and Sustainability of District-Scale Ground Coupled Heat Pump Systems. Geotechnical and Geological Engineering, 35(2), (2017), 1–14.

Raymond, J. and Lamarche, L.: Simulation of Thermal Response Tests in a Layered Subsurface. Applied Engineering, 109, (2013), 293–301.

Siliski, A., Florea, L.J., Dowling, C.B., Neumann, K., Samuelson, A., Marsha, D.: Petrographic and Hydrogeologic Investigations for a District-scale Ground-coupled Heat Pump-Ball State University. Book Chapter in Geothermal Energy: An Important Resource, edited by G. R. Osinski and D. A. Kring, The Geological Society of America, Indiana. (2016).

Tyler, S.W., Selker, J.S., Hausner, M.B., Hatch, C.E., Torgersen, T., Thodal, C.E., and Schladow, S.G.: Environmental Temperature Sensing using Raman Spectra DTS Fiber-optic Methods. Water Resources Research, 45, (2009), W00D23.

Walker, M.D., Meyer, L.L., Tinjum, J.M., and Hart, D.J.: Thermal Property Measurements of Stratigraphic Units with Modeled Implications for Expected Performance of Vertical Ground Source Heat Pumps. Geotechnical and Geological Engineering, 33(2), (2015), 223–238.